Simulation of the behaviour of FCC polycrystals during reversed torsion

Wu, P.D.; Neale, K.W.; van der Giessen, E.

Published in:
International Journal of Plasticity

DOI:
10.1016/S0749-6419(96)00048-4

Publication date:
1996

Pergamon

International Journal of Plasticity, Vol. 12, No. 9, pp. 1199–1219, 1996

0749-6419/96 $15.00 + .00

PII: S0749-6419(96)00048-4

SIMULATION OF THE BEHAVIOUR OF FCC POLYCRYSTALS DURING REVERSED TORSION

P. D. Wu,[1] K. W. Neale[1] and E. Van der Giessen[2]

[1]University of Sherbrooke, Department of Civil Engineering, Sherbrooke, Quebec, Canada J1K 2R1

[2]Delft University of Technology, Lab. for Engineering Mechanics, Mekelweg 2, 2628 CD Delft, The Netherlands

(*Received in final revised form* 13 *July* 1996)

Abstract—Taylor-type polycrystal plasticity models with various single slip hardening laws are evaluated by studying the large strain behaviour of FCC polycrystals during reversed torsion. The hardening laws considered include the model of Asaro and Needleman ("Texture Development and Strain Hardening in Rate Dependent Polycrystals," Acta Metall. (1985), **34**, 1553) as well as a power-law and an exponential version of that, and a more recent model by Bassani and Wu ("Latent Hardening in Single Crystals II. Analytical Characterization and Predictions," Proc. R. Soc. Lond. (1991), **A435**, 21). The material parameters for the various hardening laws are fitted to experimental compression data for copper and then used to predict reversed large strain torsion of tubes. Differences under "free-end" (axially unconstrained) or "fixed-end" (axially constrained) conditions between predictions and experimental observations are discussed in detail. In addition to the torque response, the Swift effects upon twist reversal are studied. Copyright © 1997 Elsevier Science Ltd

I. INTRODUCTION

It is widely recognized that the deformation of polycrystals under large plastic strains results in the reorientation of individual grains into preferred orientations to form textures. Textured polycrystals have anisotropic mechanical and physical properties, which are of well-known importance in forming processes such as rolling and deep drawing.

Asaro and Needleman [1985] have developed an elastic–plastic, rate-dependent polycrystalline model in which plastic deformation within the individual crystals is taken to be by crystallographic slip alone. To present the global response of the polycrystal, they follow the pioneering work of Taylor and assume that all grains have equal volume, and that the deformation gradient within each grain has a uniform value throughout the aggregate. In this Taylor-type model, the macroscopic Cauchy stress in the polycrystal is simply the average of the Cauchy stress over all grains, and compatibility is satisfied and equilibrium holds in each crystal, but equilibrium is usually violated between crystals.

Based on the work of Brown *et al.* [1989], Anand and co-workers (see e.g. Kalidindi *et al.* [1992] and Bronkhorst *et al.* [1992]) consider a specific form of the constitutive function for the single slip hardening rate and thus develop a slightly modified form of the Taylor-type model of Asaro and Needleman [1985].

Apart from the description of hardening on a particular slip system due to slip on that system (self-hardening), the latent hardening of slip systems due to slip on other systems is an important issue. An approach that has been widely adopted is to assume that the hardening on any slip system is independent of the slip on other systems and, thereby, incorporates only a limited coupling between slip systems. As a consequence, this simple description cannot account for the significant differences in overall hardening observed for different orientations of the tensile axis (see e.g. Wu *et al.* [1991]). Based on this and other observations, and the recent experiments of Wu *et al.* [1991], Bassani and Wu [1991] have developed a new analytical characterization for the evolution of the complete set of instantaneous hardening moduli for a single crystal undergoing multiple slip plastic deformation. Various behaviours predicted by the model for FCC single crystals (copper) were found to be in good agreement with experimental observations (Bassani [1994]). It is noted that the Bassani–Wu model is essentially a rate-independent single crystal plasticity model; in this paper, we employ it in a rate-dependent Taylor-type polycrystal model.

Although the recent advances in the single slip hardening models provide a foundation for further understanding of the large strain behaviour of polycrystals, evaluation of the constitutive models is far from sufficient. First of all, there is no comparison of predicted large strain behaviour between various Taylor-type models with different single slip hardening laws. Secondly, there is no detailed comparison of predictions based on the models, except for the Anand model, against actual experimental data (see e.g. Kalidindi *et al.* [1992] and Bronkhorst *et al.* [1992]).

The purpose of this paper is to evaluate various Taylor-type models with different single slip hardening laws by mainly studying the differences in predicted large strain reverse torsion behaviour. Torsion of a circular bar in the range of large plastic strains has recently been the subject of numerous investigations (see e.g. Harren *et al.* [1989]). One of the main reasons for this is that the torsion test provides an excellent means for obtaining experimental data for the constitutive behaviour of elastic–plastic solids at large to very large deformations. The major advantage over the standard tensile test is that deformations of a circular bar in torsion remain axially homogeneous up to final failure without showing strain localization phenomena such as necking and shear banding. Evidently, torsional deformations are inhomogeneous in the radial direction, but this multiaxiality is lower and more tractable than the three-dimensional state inside a neck. Furthermore, it is well-known that the axial stress development during fixed-end torsion and the axial elongation during free-end torsion in initially isotropic polycrystalline metals are mainly due to texture development. The predictions of these second-order phenomena depend strongly on the constitutive model — in particular the description of anisotropic hardening (see e.g. Harren *et al.* [1989]). Thus, the torsion test seems to provide an effective means for assessing the adequacy of constitutive models.

Some authors have studied the large strain torsion of thin-walled tubes using crystal plasticity models (see e.g. Harren *et al.* [1989]; Lowe & Lipkin [1991]; Lin & Havner [1996]) in terms of simple homogeneous shear type of deformation processes. Reducing the wall thickness of a tube will reduce the nonuniformity of the deformation, and if the tubes are extremely thin then the deformation can be approximated to be homogeneous so that the experimental results can be easily interpreted. In fact, many experimental procedures based on torsion have used thin-walled tubes for which the state of the deformation has been assumed to be completely uniform and, for axially constrained or "fixed-end" torsion, to be a state of simple shear (see e.g. Field & Adams [1990]). Unfortunately, in

order to avoid buckling in a finite deformation torsion experiment on a hollow tube, it is necessary that the thickness of the tube be at least 10–15% of the mean radius (Khen & Rubin [1992]). These hollow tubes cannot really be considered to be thin and the deformation is not really homogeneous (Wu & Van der Giessen [1993]). Therefore, those torsion analyses mentioned above cannot predict the observed phenomena in solid bars and thick-walled tubes, since they do not account for the inhomogeneity of the stress and deformation states in the specimen. It is only recently that Neale *et al.* [1990] have presented a first accurate analysis of fixed-end torsion of a solid bar using a rigid plastic version of the Taylor polycrystal model. Their analysis is based on a special solution procedure which constructs the solution from the response to simple shear. It is noted that this special solution procedure cannot account for the effect of elasticity, which can influence the plastic response of a polycrystal during finite strain deformation following a strain path change, even during homogeneous deformation (Lowe & Lipkin [1991]). Very recently, Van der Giessen *et al.* [1992a] adopt a numerical procedure employing the special purpose finite elements designed by Wu and Van der Giessen [1991]. With this numerical tool, they were able to study large strain behaviour of fixed-end torsion and free-end torsion of solid bars. In the present paper, the numerical method is further extended to simulate large strain torsion of circular cylinders from a very thin-walled tube to a solid bar.

The plan of this paper is as follows. In Section II, we briefly review the constitutive models with the emphasis on different single slip hardening laws. The torsion problem formulation and the method of solution are presented in Section III. We begin Section IV by estimating the hardening parameters by curve-fitting numerical simulations of uniaxial compression using various Taylor-type models to corresponding experimental data found in the literature. These hardening parameters are then used to predict large strain behaviour during reversed torsion. Differences between models in predictions as well as the differences between predicted behaviour and experimental observations are emphasized. The discussion and conclusion are presented in Section V.

Tensors and vectors will be denoted by bold letters. The tensor product is denoted by $\otimes$ and the following operation for second-order tensors applies ($\mathbf{a} = a_{ij}\mathbf{e}_i \otimes \mathbf{e}_j$, $\mathbf{b} = b_{ij}\mathbf{e}_i \otimes \mathbf{e}_j$, $\mathbf{e}_i$ being a Cartesian basis): $\mathbf{ab} = a_{ik}b_{kj} \otimes \mathbf{e}_j$, $\mathbf{a} \cdot \mathbf{b} = a_{ij}b_{ij}$, with proper extension to high-order tensors. Superscripts T and -1 denote the transverse and inverse of a second-order tensor, respectively. The trace is denoted by tr.

II. CONSTITUTIVE MODELS

We now briefly recapitulate the constitutive models employed in this paper. For details we refer to Asaro and Needleman [1985], Kalidindi *et al.* [1992] and Bassani [1994].

The total deformation of a crystallite is the result of two distinct physical mechanisms: crystallographic slip due to dislocation motion on the active slip systems, and elastic lattice distortion. We consider FCC crystals having the usual $\{111\}<110>$ slip systems where the slip planes are the $\{111\}$ crystallographic planes with normals $\mathbf{m}$, and the $<110>$ directions are shear directions with slip vectors $\mathbf{s}$. Plastic deformation of the crystal is envisaged to occur as a set of plastic simple shears along the various slip systems, leaving the lattice and the slip systems' vectors ($\mathbf{s}_\alpha$, $\mathbf{m}_\alpha$) not only essentially undistorted but also unrotated. Next, the material and lattice are considered to deform elastically and

rotate rigidly from the plastically deformed state to the current configuration. Accordingly, we have the following decomposition for the deformation gradient tensor $\mathbf{F}$

$$\mathbf{F} = \mathbf{F}^*\mathbf{F}^p, \tag{1}$$

where $\mathbf{F}^p$ consists solely of crystallographic slipping along specific slip systems, and $\mathbf{F}^*$ includes the elastic distortion and any rigid body rotations. From eqn (1) the spatial gradients of velocity are

$$\mathbf{L} = \dot{\mathbf{F}}\mathbf{F}^{-1} = \mathbf{L}^* + \mathbf{L}^p, \tag{2}$$

where,

$$\mathbf{L}^* = \dot{\mathbf{F}}^*\mathbf{F}^{-1}, \qquad \mathbf{L}^p = \mathbf{F}^*(\dot{\mathbf{F}}^p\mathbf{F}^{p-1})\mathbf{F}^{*-1}. \tag{3}$$

Taking symmetric and antisymmetric parts of the above relations leads to the elastic and plastic strain rate $\mathbf{D}^*$ and $\mathbf{D}^p$, the so-called plastic spin $\mathbf{W}^p$, and the spin $\mathbf{W}^*$ associated with the rigid lattice rotation:

$$\mathbf{D} = \mathbf{D}^* + \mathbf{D}^p, \qquad \mathbf{W} = \mathbf{W}^* + \mathbf{W}^p. \tag{4}$$

Since $\mathbf{s}_\alpha$ and $\mathbf{m}_\alpha$ are regarded as lattice vectors, they are stretched and rotated as follows

$$\mathbf{s}_\alpha^* = \mathbf{F}^*\mathbf{s}_\alpha, \qquad \mathbf{m}_\alpha^* = \mathbf{m}_\alpha\mathbf{F}^{*-1}.$$

The vectors $\mathbf{s}_\alpha^*$ and $\mathbf{m}_\alpha^*$, orthogonal since $\mathbf{s}_\alpha$ and $\mathbf{m}_\alpha$ are, characterize a particular slip system in the current state. Their evolution is characterized by

$$\dot{\mathbf{s}}_\alpha^* = \mathbf{L}^*\mathbf{s}_\alpha^*, \qquad \dot{\mathbf{m}}_\alpha^* = -\mathbf{L}^{*T}\mathbf{m}_\alpha^*.$$

By introducing the following symmetric and antisymmetric tensors, respectively, for each slip system α:

$$\mathbf{P}_\alpha = \frac{1}{2}(\mathbf{s}_\alpha^* \otimes \mathbf{m}_\alpha^* + \mathbf{m}_\alpha^* \otimes \mathbf{s}_\alpha^*), \qquad \mathbf{W}_\alpha = \frac{1}{2}(\mathbf{s}_\alpha^* \otimes \mathbf{m}_\alpha^* - \mathbf{m}_\alpha^* \otimes \mathbf{s}_\alpha^*), \tag{5}$$

the plastic strain-rate and spin for the crystal can be written as:

$$\mathbf{D}^p = \sum_\alpha \mathbf{P}_\alpha\dot{\gamma}_\alpha, \qquad \mathbf{W}^p = \sum_\alpha \mathbf{W}_\alpha\dot{\gamma}_\alpha, \tag{6}$$

where $\dot{\gamma}_\alpha$ is the shear rate on the slip system α. The elastic constitutive equation for a crystal is specified by

$$\overset{\nabla}{\boldsymbol{\tau}}{}^* = \dot{\boldsymbol{\tau}} - \mathbf{W}^*\boldsymbol{\tau} + \boldsymbol{\tau}\mathbf{W}^* = \mathcal{L}\mathbf{D}^* \tag{7}$$

where $\overset{\nabla}{\boldsymbol{\tau}}{}^*$ is the Jaumann rate of the Kirchhoff stress tensor based on the lattice rotations, and $\mathcal{L}$ represents the elastic moduli. These moduli are based on the anisotropic elastic constants of the FCC crystal and thus exhibit the appropriate cubic symmetry.

In order to express the constitutive equation (7) in terms of the Jaumann rate of Cauchy stress $\overset{\nabla}{\boldsymbol{\sigma}}$ ($\boldsymbol{\tau} = \det(\mathbf{F})\boldsymbol{\sigma}$), based on the continuum spin $\mathbf{W}$, we introduce a second-order tensor $\mathbf{R}_\alpha$ for each slip system as follows:

$$\mathbf{R}_\alpha = \mathcal{L}\mathbf{P}_\alpha + \mathbf{W}_\alpha\boldsymbol{\sigma} - \boldsymbol{\sigma}\mathbf{W}_\alpha. \tag{8}$$

Using eqns (4)–(6) and (8), the constitutive equation (7) can be rewritten in the form

$$\overset{\nabla}{\boldsymbol{\sigma}} = \mathcal{L}\mathbf{D} - \dot{\boldsymbol{\sigma}}^0 - \boldsymbol{\sigma}\,\mathrm{tr}\,\mathbf{D}, \tag{9}$$

where $\dot{\boldsymbol{\sigma}}^0$ is a visco-plastic type stress rate defined by

$$\dot{\boldsymbol{\sigma}}^0 = \sum_\alpha \mathbf{R}_\alpha\dot{\gamma}_\alpha. \tag{10}$$

The slip rates are taken to be governed by the power-law expression

$$\dot{\gamma}_\alpha = \dot{\gamma}_0\,\mathrm{sgn}\,\tau_\alpha\left|\frac{\tau_\alpha}{g_\alpha}\right|^{1/m}, \tag{11}$$

where τ_α is the resolved shear stress on slip system α and g_α is its hardness; m is the strain-rate sensitivity index and $\dot{\gamma}_0$ is a reference shear rate. The resolved shear stress is related to the Cauchy stress through

$$\tau_\alpha = \mathbf{P}_\alpha \cdot \boldsymbol{\sigma}. \tag{12}$$

The g_α characterize the current strain hardened state of the crystal. For multiple slip, the evolution of the hardness is governed by

$$\dot{g}_\alpha = \sum_\beta h_{\alpha\beta}\,|\,\dot{\gamma}_\beta\,|. \tag{13}$$

where $g_\alpha(0)$ is the initial hardness and is taken to be a constant τ_0 for each slip system, and where $h_{\alpha\beta}$ are the hardening moduli. The form of the moduli is

$$h_{\alpha\beta} = q_{\alpha\beta}h_\beta \qquad (\text{no sum on } \beta), \tag{14}$$

where h_β is a single slip hardening rate, and $q_{\alpha\beta}$ is the matrix describing the latent hardening behaviour of the crystallite. For FCC crystals with 12 slip systems, we take $q_{\alpha\beta}$, as in Asaro and Needleman [1985], to be given by

$$q_{\alpha\beta} = \begin{bmatrix} \mathbf{A} & q\mathbf{A} & q\mathbf{A} & q\mathbf{A} \\ q\mathbf{A} & \mathbf{A} & q\mathbf{A} & q\mathbf{A} \\ q\mathbf{A} & q\mathbf{A} & \mathbf{A} & q\mathbf{A} \\ q\mathbf{A} & q\mathbf{A} & q\mathbf{A} & \mathbf{A} \end{bmatrix}$$

where q is the ratio of the latent hardening rate to self hardening rate, and A is a 3×3 matrix fully populated by ones. In the above, slip systems {1,2,3} are coplanar, as are systems {4,5,6}, {7,8,9} and {10,11,12}. Thus the ratio of the latent hardening rate to the self hardening rate for coplanar systems is taken as unity.

Asaro and Needleman [1985], among others, simply take each g_α to depend on the accumulated sum, γ_a, of the slips; i.e.

$$g_\alpha = g_\alpha(\gamma_a) \tag{15}$$

where

$$\gamma_a = \int_0^t \sum_\alpha |\dot{\gamma}_\alpha| \, dt. \tag{16}$$

Thus, h_β is identical for each system β.

Based on measurements of strain hardening of single crystals of aluminium alloys by Chang and Asaro [1981], the following single slip hardening rate was used by Asaro and co-workers (see e.g. Harren *et al.* [1989]):

$$h_\beta = h_s + (h_0 - h_s) \operatorname{sech}^2 \left\{ \left(\frac{h_0 - h_s}{\tau_s - \tau_0} \right) \gamma_a \right\} \tag{17}$$

where h_0 and h_s are the system's initial and asymptotic hardening rates. If $h_s = 0$, then τ_s represents the saturation value of the shear stress. Another single slip hardening law employed in this paper takes an exponential form for the hardening rate on all slip systems, i.e.

$$h_\beta = \frac{\tau_s - \tau_0}{\gamma_0} \exp\left(\frac{\gamma_a}{\gamma_0} \right). \tag{18}$$

Motivated by the work of Brown *et al.* [1989], Anand and co-workers (see e.g. Kalidindi *et al.* [1992] and Bronkhorst *et al.* [1992]) have considered the following power-law form of the constitutive function h_β

$$h_\beta = h_0 \left(1 - \frac{g_\beta}{\tau_s} \right)^a, \tag{19}$$

where h_0, a and τ_s are slip system hardening parameters which are taken to be identical for all slip systems. Unlike the Asaro (17) or the exponential (18) single slip hardening rate, h_β in eqn (19) is directly related to the current hardness g_β of the slip system.

As pointed out before, the simple form for $h_{\alpha\beta}$ in eqn (14) incorporates only a limited coupling between slip systems through off-diagonal components that scale by the latent hardening parameter q with corresponding diagonal components. When viewed in terms of observations from uniaxial stressing of single crystals including orientation dependence of hardening, secondary slips before overshoot and coarse slip band formation, the degree of latent hardening introduced in eqn (14) appears to be too high. By reviewing reported experimental observations and reinterpreting latent hardening, Bassani and Wu [1991]

proposed a particular multiplicative form in which each diagonal component is taken as the product of a self-hardening term h and an interactive hardening term G:

$$h_{\alpha\alpha} = h(\gamma_\alpha)G. \tag{20}$$

The hardening of system β due to slip on system α is simply taken to be a fraction q of the active modulus, and the off-diagonal components are given by

$$h_{\beta\alpha} = qh_\alpha, \qquad \alpha \neq \beta. \tag{21}$$

It is clear that Asaro and co-workers as well as others have adopted a hardening description that is a special case of the form (20) where $G = 1$. A form for G that equals unity when its arguments are all zero and approaches asymptotically to finite values when all slips $\gamma_\beta(\beta \neq \alpha)$ are large is (Bassani & Wu [1991])

$$G = 1 + \sum_{\beta \neq \alpha} f_{\alpha\beta} \tanh\left(\frac{\gamma_\beta}{\gamma_0}\right), \tag{22}$$

where γ_0 represents the amount of slip after which a given interaction between slip systems α and β reaches peak strength. Each $f_{\alpha\beta}$ represents the strength of the interaction and depends on the type of dislocation junction formed between slip system α and β, which in turn depends on the geometric relation between the two slip systems. For FCC crystals, Bassani and Wu [1991] classify $f_{\alpha\beta}$ into five groups. Table 2 in Bassani and Wu [1991] gives each value of $f_{\alpha\beta}$, while the corresponding notations for the slip systems and slip planes are given in their Table 1.

A simple form for the self-hardening $h(\gamma_\alpha)$ that gives a monotonically decreasing modulus at small strains and a finite rate of hardening at large γ_α is (Bassani and Wu [1991])

$$h(\gamma_\alpha) = h_s + (h_0 - h_s)\,\mathrm{sech}^2\left\{\left(\frac{h_0 - h_s}{\tau_I - \tau_0}\right)\gamma_\alpha\right\}, \tag{23}$$

where τ_0 is the initial critical resolved shear stress, τ_I is the so-called stage I stress and h_0 is the initial hardening rate, and h_s is assumed to depend on the total accumulated slip γ_a on all slip systems (Bassani [1994]):

$$h_s = h_s^I + (h_s^{III} - h_s^I)\tanh\left(\frac{\gamma_a}{\gamma_0^{III}}\right), \tag{24}$$

where h_s^I and h_s^{III} are the hardening rates during stage I and stage III, respectively, and γ_0^{III} is approximately the accumulated slip at the onset of stage III. It is important to note, especially for the application to reverse loading histories, that the slip rates $\dot{\gamma}_\alpha$ in the present description in eqns (6)–(14) can be either positive or negative (contrary to Bassani [1994]). It is implied in the hardening law (20)–(23) that γ_α is the accumulated shear on the particular slip system α, i.e. $\int |\dot{\gamma}_\alpha|\,dt$. Equation (23) is similar in form to eqn (17), but is a function of the slip system's accumulated shear instead of the total accumulated shear on all slip systems.

The response of a polycrystal comprised of many grains is obtained by invoking the Taylor assumption. Thus, at a material point representing a polycrystal of N grains, the deformation in each grain is taken to be identical to the macroscopic deformation of the continuum. Furthermore, the macroscopic values of all quantities such as stresses, stress rates, and elastic moduli are obtained by averaging their respective values over the total number of grains at the particular material point.

III. PROBLEM FORMULATION AND METHOD OF SOLUTION

We consider a uniform circular cylindrical tube of initial outer radius R_{o0}, initial inner radius R_{i0}, and initial length L_0, which is subject to a twist φ due to an applied torque T. Also, the tube may be subjected simultaneously to an axial force F associated with an axial displacement U, while the lateral surfaces remain traction free. All properties are assumed to be axisymmetric and homogeneous along the axial direction. Although anisotropy due to texture evolution is induced during the deformation process, the behaviour remains axisymmetric and is further assumed to remain uniform in the axial direction. Thus, we neglect the formation and propagation of macroscopic circumferential shear bands that may develop. Consequently, the tube remains circular cylindrical, and at the current deformed state has an outer radius R_0, an inner radius R_i, and a length L. The end faces of the tube are constrained such that they remain plane and perpendicular to the axial direction.

The kinematics of the problem is readily established with the aid of a spatially fixed cylindrical coordinate system $x^i = (r, \theta, z)$ with associated orthonormal base vectors $\mathbf{e}_i$. These base vectors are associated with material elements in their current deformed state, so that tensor components with respect to this basis represent physical components. If the initial cylindrical coordinates of a material point are $x_0^i = (r_0, \theta_0, z_0)$, its coordinates in a deformed configuration at time t are assumed to be given by

$$x^i = (r, \theta, z) = (r(r_0, t),\ \theta_0 + \psi(t) z_0,\ e(t) z_0), \tag{25}$$

with $\psi = \varphi / L_0$ the twist per unit initial length L_0, and with $e = L/L_0$ the extensional stretch in axial direction. The components of the strain-rate tensor D_{ij} and the spin tensor W_{ij} are obtained as

$$D_{11} = \frac{\partial \dot{r}}{\partial r}, \quad D_{22} = \frac{\dot{r}}{r}, \quad D_{33} = \frac{\dot{e}}{e}, \quad D_{23} = \frac{1}{2} \frac{r\dot{\psi}}{e}, \quad D_{12} = D_{13} = 0; \tag{26}$$

$$W_{12} = -\frac{z\dot{\psi}}{e}, \quad W_{13} = 0, \quad W_{23} = \frac{1}{2} \frac{r\dot{\psi}}{e}, \tag{27}$$

respectively.

Regarding the stress state inside the tube, axisymmetry and axial homogeneity imply that the components of the Cauchy stress tensor depend only on the radial coordinate, $\sigma_{ij} = \sigma_{ij}(r)$, while $\sigma_{13} = 0$. For isotropic materials and for orthotropic materials with their principal axes along the x^i, one also has $\sigma_{12} = 0$; with the constitutive models discussed above this depends on the initial texture and cannot be guaranteed, but the

actual value of σ_{12} is of no concern for the solution of the problem at hand. The resultant torque T and the axial force F are given by

$$T = 2\pi \int_{R_i}^{R_o} r^2 \sigma_{23}\, dr, \qquad F = 2\pi \int_{R_i}^{R_o} r\sigma_{33}\, dr \tag{28}$$

while the lateral surfaces are traction-free, $\sigma_{11}(R_i) = 0$ and $\sigma_{11}(R_o) = 0$. Free-end torsion is analyzed by specifying the boundary condition $F = 0$, while fixed-end torsion follows from the condition $\dot{e} = 0$.

It is clear from the above considerations that the torsion problem is basically a one-dimensional problem along the radial coordinate r. This problem can be dealt with in an efficient way by means of special purpose finite elements in the radial direction designed by Wu and Van der Giessen [1991]. As shown schematically in Fig. 1(a), each element is actually a circular cylindrical tube, with inner radius r_1 and outer radius r_2 in the current configuration. Such an element is geometrically one-dimensional along the r-axis, with two nodes at $r = r_1$ and $r = r_2$, respectively (see Fig. 1(b)). Within each element the radial velocity $v_1 = \dot{r}_1$ is interpolated through a linear interpolation of the circumferential strain-rate $D_{22} = \dot{r}/r$ between the nodal values $\dot{r}_1/r_1$ and $\dot{r}_2/r_2$. The degrees of freedom of the entire finite element model of the tube consisting of, say, n elements then comprise $n + 1$ radial nodal displacements along with the axial displacement U and the twist φ. Furthermore, each element has two material sampling points whose positions coincide with the Gauss point. For more details concerning the precise formation of the finite element equations, we refer to Wu and Van der Giessen [1991].

In the present study, the constitutive models implemented are the elastic–viscoplastic polycrystal models with the various different single slip hardening laws presented earlier. Each material sampling point in the finite element formulation is modelled as a polycrystalline aggregate consisting of N grains, and the Taylor assumption is applied locally at each point. The polycrystal constitutive equations are implemented via the one-step, explicit rate tangent method described by Peirce *et al.* [1984]. Moreover, an adaptive time stepping method developed by Van der Giessen and Neale [1993] is used. Finally, an equilibrium correction procedure is applied to prevent drifting of the solution from the

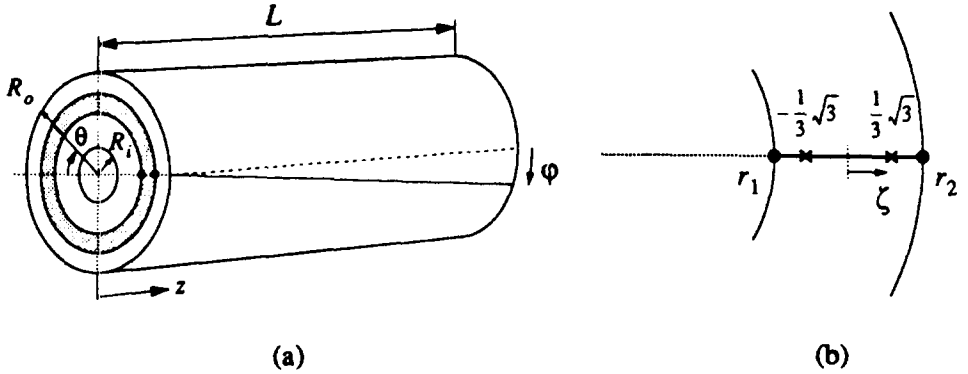

Fig. 1. The finite elements used here are cylindrical tubes with inner radius r_1 and outer radius r_2; (a) definition of nodal points (x) and (b) material sampling points (•).

true equilibrium path. For more details concerning the time-integration scheme adopted, we refer to Van der Giessen and Neale [1993].

IV. RESULTS

The material we study is annealed OFHC copper with the standard values of elastic constants $C_{11} = 170$ GPa, $C_{12} = 124$ GPa and $C_{44} = 75$ GPa at room temperature (Simmons & Wang [1971]). The slip system reference plastic shearing rate is taken as $\dot{\gamma}_0 = 0.001\ s^{-1}$, while the slip rate sensitivity parameter m is assumed to be equal to the macroscopic strain rate sensitivity determined by Kalidindi *et al.* [1992], that is $m = 0.012$. Bassani and Wu [1991] found that excellent agreement with experimental observations in FCC single crystals (copper) is obtained with the latent hardening parameter $q = 0$ in their model; therefore, here also we assume $q = 0$ for the Bassani–Wu model (partly because of lack of sufficient experimental data). A set of 400 crystal orientations is used in our simulations to represent the initial isotropic texture in the undeformed copper. The distribution of this initial texture is constructed from a random distribution consisting of 100 grains, which is then symmetrized with respect to the $r-\theta$ and $\theta-z$ planes (see Fig. 2). The corresponding average elastic modulus tensor then is orthotropic for deformations according to eqns (26) and (27) but not exactly isotropic (see Van der Giessen & Neale [1993]).

We estimate the hardening parameters in the constitutive models by curve-fitting numerical simulations of uniaxial compression to corresponding experimental data given by Kalidindi *et al.* [1992]. The uniaxial compression process in our numerical calculations is characterized by the spatial gradients of velocity:

$$\mathbf{L} = \dot{\varepsilon}\mathbf{e}_3 \otimes \mathbf{e}_3 + \dot{\varepsilon}_\perp \mathbf{e}_2 \otimes \mathbf{e}_2 + \dot{\varepsilon}_\perp \mathbf{e}_1 \otimes \mathbf{e}_1 \tag{29}$$

with $\dot{\varepsilon} = -0.001\ s^{-1}$ and $\dot{\varepsilon}_\perp$ to be determined by invoking the boundary condition $\sigma_{22} = 0$. It is found that this *axisymmetric* compression with the boundary condition results in $\sigma_{11} \neq 0$ because the average elastic modulus tensor is orthotropic for general 3D deformations. Nevertheless, the magnitude of σ_{11} is two orders of magnitude smaller than the applied compressive stress $\sigma = \sigma_{33}$. The shear stresses are essentially zero.

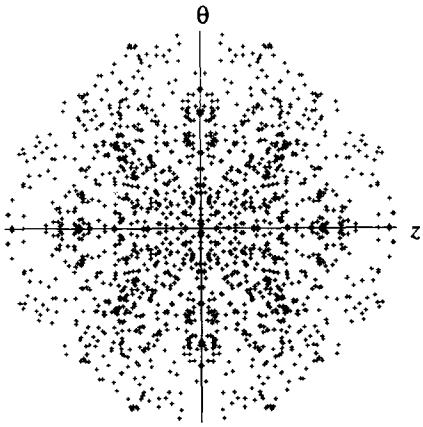

Fig. 2. Initial grain orientation distribution represented by {111} stereographic pole figure for 400 grains.

The values of the material parameters are:

Asaro hardening: $\tau_0 = 16$ MPa, $\tau_s/\tau_0 = 4.4$, $h_0/\tau_0 = 8.25$, $h_s/\tau_o = 0.48$, $q = 1.4$;
Exponential hardening: $\tau_0 = 16$ MPa, $\tau_s/\tau_0 = 7.65$, $\gamma_0 = 0.75$, $q = 1.0$;
Anand hardening: $\tau_0 = 16$ MPa, $\tau_s/\tau_0 = 9.25$, $h_0/\tau_0 = 11.25$, $\alpha = 2.25$, $q = 1.4$;
Bassani–Wu hardening: $\tau_0 = 1$ MPa, $\tau_s/\tau_0 = 1.3$, $h_0/\tau_0 = 90$, $h_s^I/\tau_0 = 4.45$, $h_s^{III}/\tau_0 = 0.15$, $\gamma_0 = 0.001$, $\gamma_0^{III} = 1.75$, $q = 0$.

It is noted that our estimated values of hardening parameters for Anand hardening are the same as those estimated by Kalidindi *et al.* [1992]. The correspondences between the calculated responses based on different models and the experimental data are presented in Fig. 3. The curve-fits are reasonable. We have also tried to fit the exponential hardening with $q = 1.4$, and found that the exponential hardening model with $q = 1.4$ cannot accurately simulate the uniaxial compression test of the OFHC copper; therefore, we used $q = 1.0$.

We proceed by numerically simulating the large strain behaviour of OFHC copper during reversed torsion, using various Taylor-type models with different single slip hardening laws and the corresponding values of material parameters determined above.

The experimental data of large strain torsion of tubes are usually presented in terms of the following quantities:

$$\Gamma = \frac{R_{o0}}{L_0}\varphi, \qquad \bar{\tau} = \frac{3T}{2\pi(R_{o0}^3 - R_{i0}^3)}, \qquad \bar{\sigma} = \frac{F}{\pi(R_{o0}^2 - R_{i0}^2)}. \tag{30}$$

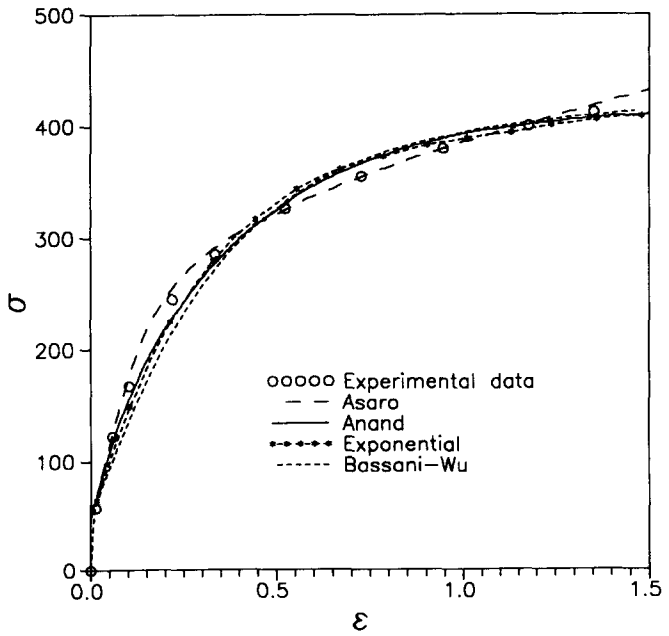

Fig. 3. Axial stress vs true strain response for uniaxial compression. The experimental data are taken from Bronkhorst *et al.* [1992].

Here, Γ represents the shear strain at the outer surface of the tube, provided that geometrical changes remain small, and $\bar{\tau}$ and $\bar{\sigma}$ are the average shear stress and axial stress across the thickness, respectively.

By comparison with semi-analytical solutions, previous investigations of solid bar torsion using macroscopic phenomenological constitutive models have shown that a uniform mesh with $n = 5$ gives a sufficiently accurate representation of the stress and strain states within that bar (Wu and Van der Giessen [1991]; Van der Giessen *et al.*, [1992b]). However, as pointed out by Wu and Van der Giessen [1993], for a tube one cannot expect to get highly accurate results using only five elements because of the intrinsic properties of the special element and the additional latent inner boundary condition $\sigma_{11}(R_i) = 0$ involved. In order to obtain sufficiently accurate results, they suggested the use of a somewhat refined mesh near the lateral surfaces (especially near the inner surface) where high strain gradients are expected. Numerical experiments show for a tube that the calculated torque and axial force as well as the shear stress distributions are not sensitive to the number of elements; but, second-order effects, such as the radial stress distribution, are indeed rather sensitive to the number of elements used. Since this paper primarily focuses on the overall characteristics of torsion (torque, axial force, elongation, etc.) which are not very sensitive to deviations from the actual stress state, we decided that a mesh comprising 10 elements with a local refinement would be sufficiently accurate.

To enable a direct comparison with experimental reverse torsion data for OFHC copper reported by Anand and Kalidindi [1994] we have taken the actual dimensions to be the same as the gauge section of the tube in Anand and Kalidindi [1994], i.e. $R_{i0} = 14.35$ mm, $R_{o0} = 15.9$ mm and $L_0 = 10.2$ mm. The applied twist rate was such that the shear strain rate $\dot{\Gamma} = 0.01\ s^{-1}$.

Figure 4 shows the predicted torque responses to fixed-end torsion of the tube and the corresponding experimental data. The experimental torque responses are softer than those from simulations especially during the forward twisting. This is mainly due to the geometry of the specimen used in experiments. We shall return to this later. The difference between Asaro hardening and others for strains smaller than 0.4 is also seen for the compression results in Fig. 3. During large strain forward twisting and the entire range of reverse twisting, Anand hardening and Asaro hardening predict a virtually identical torque response. The fact that the exponential hardening as well as the Asaro and Anand hardening models predicted different responses in forward torsion, even though their compression predictions (Fig. 3) were almost identical, may be attributed to the latent hardening effect accounted for in Asaro and Anand hardening computations. The softening predicted by the Bassani–Wu model during large strain forward twisting ($\Gamma > 0.7$) and during large strain reverse twisting ($\Gamma < 0.9$) may be due to the texture evolution as will be discussed shortly. All simulations capture most of the small Bauschinger effects observed experimentally by Anand and Kalidindi [1994]. It is noted though, that the Bauschinger effect has been found to depend on the amount of prestrain before reversal. For example, for OFHC copper under tension–compression, it has been shown by Christodoulou *et al.* [1986] that the Bauschinger effect first increases and then saturates as the prestrain is raised. However, such small strain Bauschinger effects have a different physical origin which is not incorporated in the present constitutive model.

Figure 5 shows the predicted normal stresses along with the experimental data. For the purpose of a qualitative comparison with the experimental data, the figure shows the experimental normal stress results multiplied by 9. The measured normal stress response is

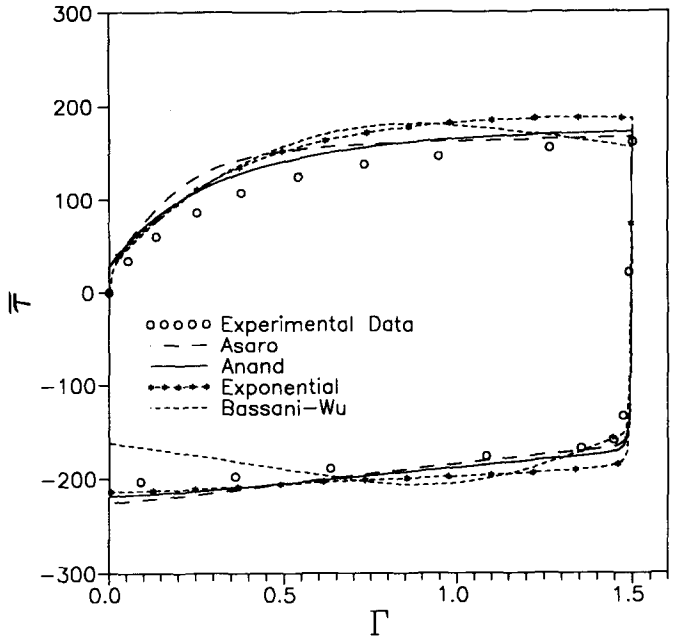

Fig. 4. Torque response to fixed-end torsion. The experimental data are taken from Anand and Kalidindi [1994].

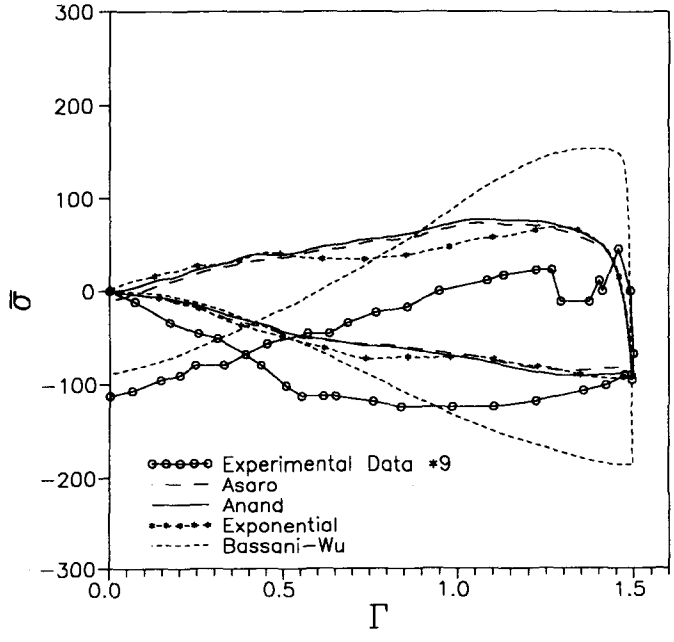

Fig. 5. Normal stress development in fixed-end torsion. The experimental data are taken from Anand and Kalidindi [1994].

compressive and increases during the forward twisting. During the transient associated with the deformation path reversal, the compressive normal stress decreases in magnitude and becomes tensile. The tensile normal stress reaches its maximum when the tube reverses to a shear strain of about 1.3. With ongoing reverse twisting the tensile normal stress decreases and once again becomes compressive. The predicted normal stresses are much larger than the experimental data in magnitude; more precisely, the predicted compressive normal stresses at $\Gamma = 1.5$ based on Asaro. Anand and exponential hardening are found to be about 8 times larger in magnitude than the experimental data, while the Bassani–Wu model predicts ever larger normal stresses. However, it is clear that only the Bassani–Wu model predicted a shape of the normal stress curve which is similar to that observed experimentally.

In order to further evaluate the constitutive models, the predicted texture evolution during large strain fixed-end torsion is examined in terms of the {111} equal-area pole figure. Figure 6 gives the predicted crystallographic textures after forward twisting to

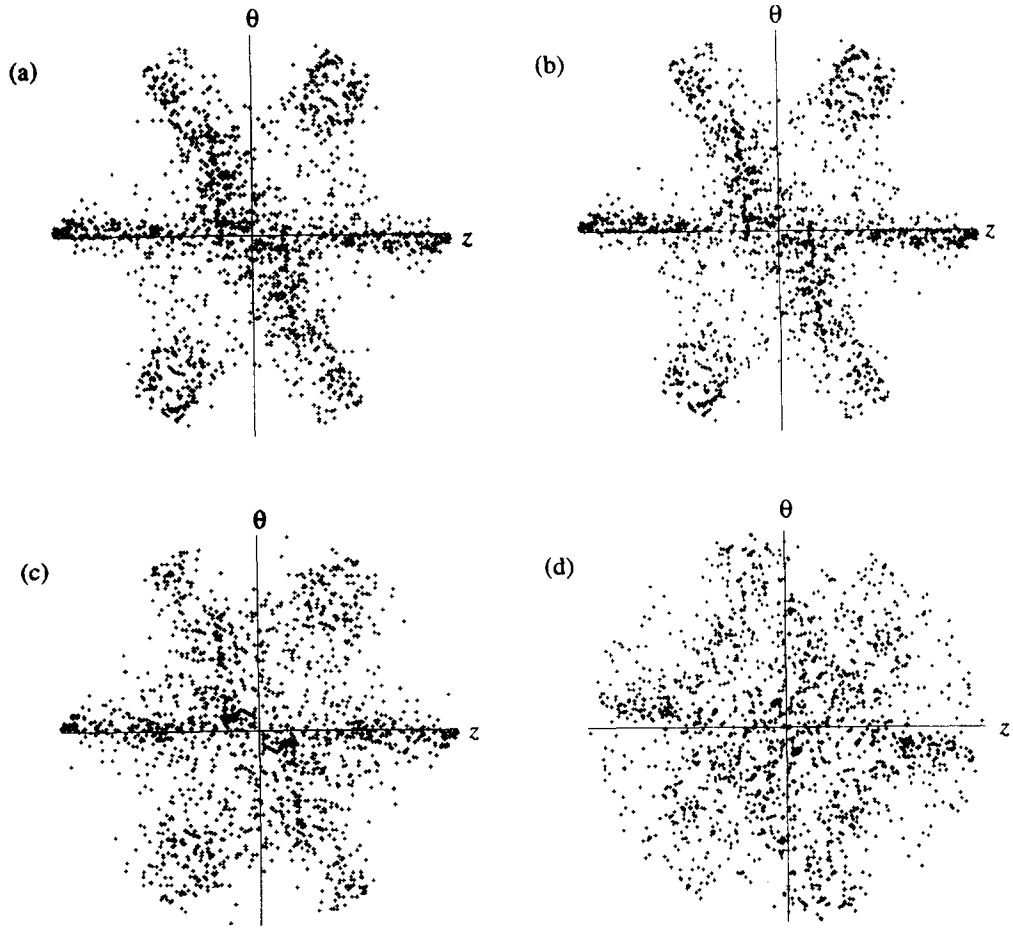

Fig. 6. Predicted {111} pole figures for fixed-end torsion after forward twisting ($\Gamma = 1.5$) based on the various hardening models: (a) Asaro, (b) Anand, (c) exponential and (d) Bassani–Wu.

$\Gamma = 1.5$. All models predict a shear texture, but with different intensities. Comparing Fig. 6 with Fig. 3 of Anand and Kalidindi [1994], it is seen that Asaro, Anand and exponential hardening based Taylor-type models predict much sharper textures than the experimental result. The differences between the exponential hardening and Asaro or Anand hardening in predicted texture at $\Gamma = 1.5$ are due to the difference between isotropic ($q = 1$) hardening and anisotropic ($q = 1.4$) hardening. It seems that the pole figure produced by Bassani–Wu hardening is relatively closer to the experimental result. The simulated pole figures after reverse twisting are shown in Fig. 7. Although the crystallographic textures according to Asaro, Anand and exponential hardening tend to return to the initial state, slight resident textures are still observed (see Figs 7(a)–(c)). In constrast, the pole figure predicted by the Bassani–Wu hardening model after complete reversal shows a strong residual shear texture (Fig. 7(d)). It seems that the texture formed during forward twisting does not tend to return to its initial state during reverse twisting, but continues its development. Another effect of reverse twisting on Bassani–Wu's prediction is a substantial

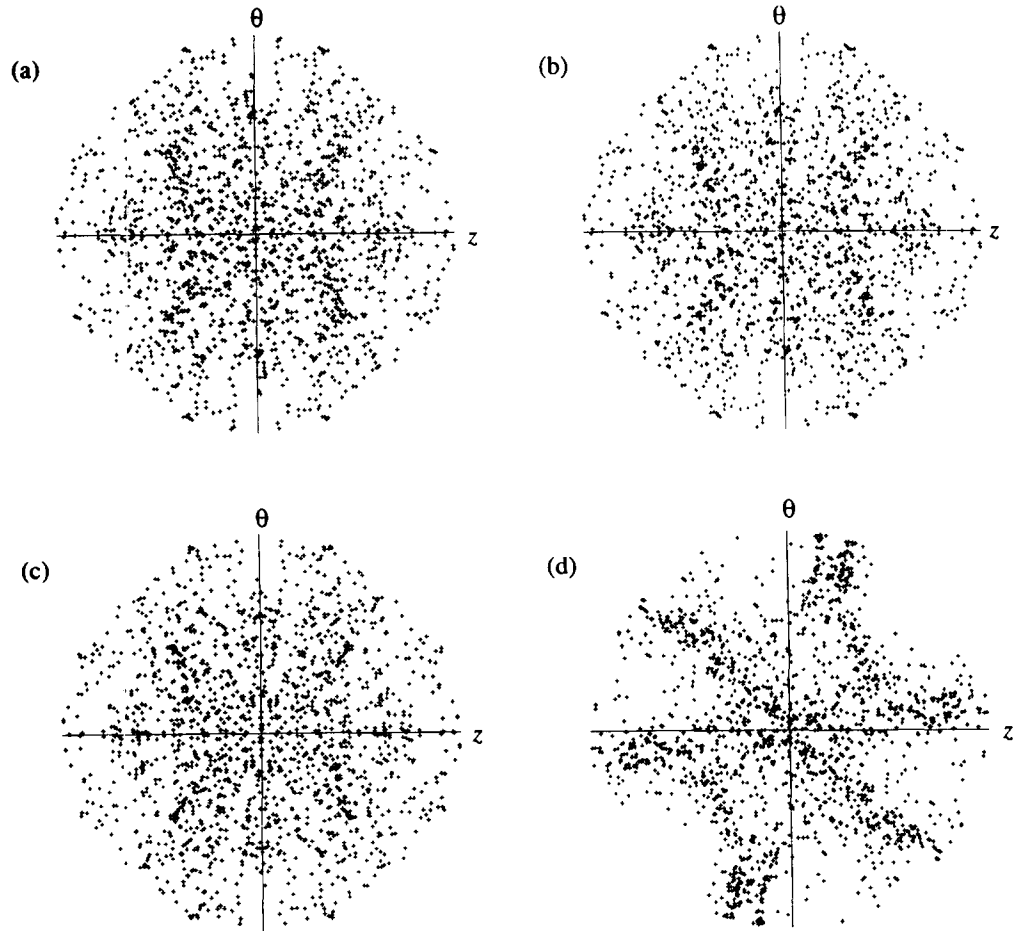

Fig. 7. Predicted {111} pole figures for fixed-end torsion after complete reverse twisting based on the various hardening models: (a) Asaro, (b) Anand, (c) exponential and (d) Bassani–Wu.

counterclockwise rotation of the texture. It seems that this kind of texture evolution results in the softening effect in torque response based on the Bassani–Wu model observed in Fig. 4.

Finally, we study the behaviour of the material during reversed free-end torsion. The boundary conditions are obtained by imposing the opposite axial boundary conditions as in the previous case of fixed-end torsion, i.e. $F = 0$, thus allowing for an axial elongation $\epsilon = \ln e$. Figures 8 and 9 give the torque response and the accompanying axial elongation development during free-end torsion. The differences between the hardening models in predicted torque are similar to that in fixed-end torsion (see Fig. 4). However, the softening effect predicted by Bassani–Wu in free-end torsion (Fig. 8) is larger than that observed in fixed-end torsion (Fig. 4). This is again due to the texture evolution according to the Bassani–Wu model as will be discussed shortly. Quite remarkably, the differences among the models in predicted axial elongation during free-end torsion (Fig. 9) are much larger than those in the predicted normal stress during fixed-end torsion (see Fig. 5). The trends of axial strain development based on Asaro, Anand and exponential hardening are similar: the specimen elongates monotonically during forward twisting, and shortens towards a constant value during reverse twisting. Based on the Bassani–Wu model, the elongated specimen after forward torsion contracts and approaches its minimum after a reverse shear strain about 0.35 ($\Gamma = 1.15$). With ongoing reverse twisting the specimen elongates again, and the axial strain increases almost linearly after a reverse strain of about 0.7 ($\Gamma = 0.8$). Furthermore, the Bassani–Wu model seems to give the best qualitative axial response (see e.g. Swift [1947]). Again qualitatively, it also corresponds well with the experiments carried out by Delhage [1990] for stainless steel solid bars. Quantitatively, the magnitudes vary considerably, however. Wu *et al.* [1996] have investigated

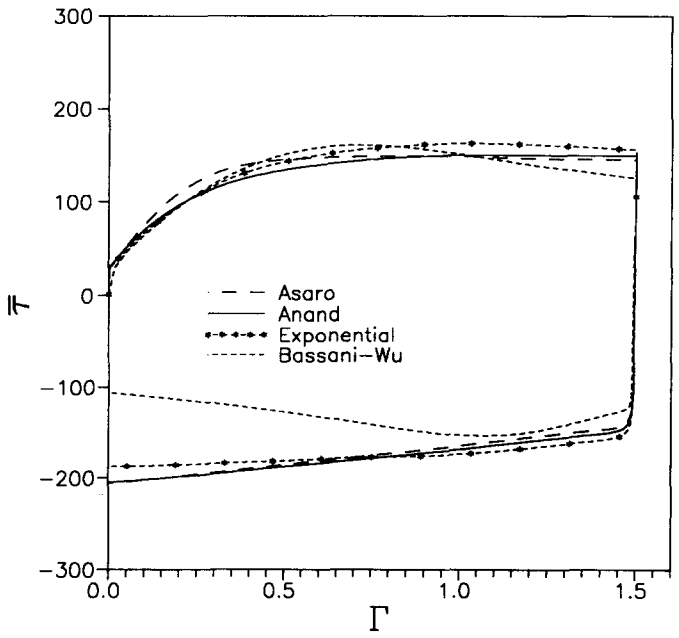

Fig. 8. Simulated torque response for free-end torsion.

the influence of the wall thickness on the Swift effect. For the tube wall-thickness used in the present study, they estimated an axial strain of 0.05 in Swift's [1947] experiment for 70–30 brass tube at $\Gamma = 1.5$. This is much smaller than the values 0.24, 0.11, 0.09 and 0.09 for, respectively, the Bassani–Wu, exponential, Asaro and Anand hardening predictions obtained here.

The predicted textures after forward twisting and after complete reverse twisting in free-end torsion are presented in Figs 10 and 11, respectively. Although the differences to fixed-end torsion can be observed, in the sense that the entire pole figures are rotated slightly about the r-axis, the results are otherwise very similar to those in fixed-end torsion (see Figs 6 and 7). Detailed comparison reveals that the predicted residual shear texture after complete reverse twisting in free-end torsion (Fig. 11) is stronger than that in fixed-end torsion (Fig. 7).

V. CONCLUSION

In this paper, the large strain behaviour of OFHC copper during reversed torsion has been numerically simulated by applying the Taylor-type polycrystal plasticity models with various different single slip hardening laws. The hardening parameters were estimated by curve-fitting numerical simulations of uniaxial compression to the corresponding experimental data.

For fixed-end torsion, the predicted results have been compared with experimental data. The experimental torque response was found to be softer than those from simulations especially during forward twisting. This is due to the geometry of the specimens used in the experimentals. Detailed finite element analyses (White [1992]) showed that the

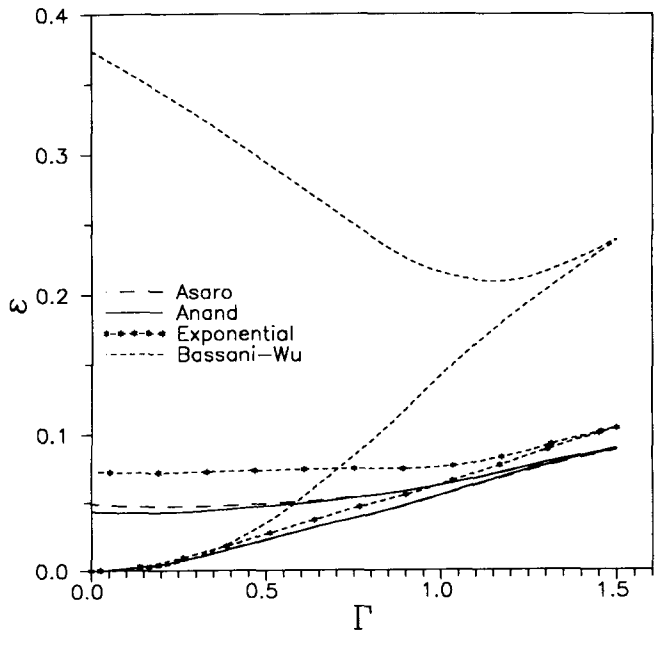

Fig. 9. Simulated axial elongation during free-end torsion.

plastic zone in the torsion specimens is not confined to the thin-walled region, but also extends into the thicker ends.

It is well known that the axial effects during torsion are very sensitive to the constitutive models. Although the predicted axial responses based on all models, especially the Bassani–Wu model, are much larger than the experimental data, the Bassani–Wu model seems to give the best qualitative axial response.

We have also studied texture evolution during reversed torsion. The Asaro, Anand and exponential hardening based Taylor-type models predicted much sharper textures after forward twisting than the experimental result. It seems that the texture predicted by the Bassani–Wu hardening model is relatively closer to the experimental result. However, the pole figure obtained for Bassani–Wu hardening after complete reversal shows a strong residual shear texture, which is just opposite to the experimental observations (Anand & Kalidindi [1994]). The softening effect in torque response based on the Bassani–Wu hardening model may be attributed to this texture evolution.

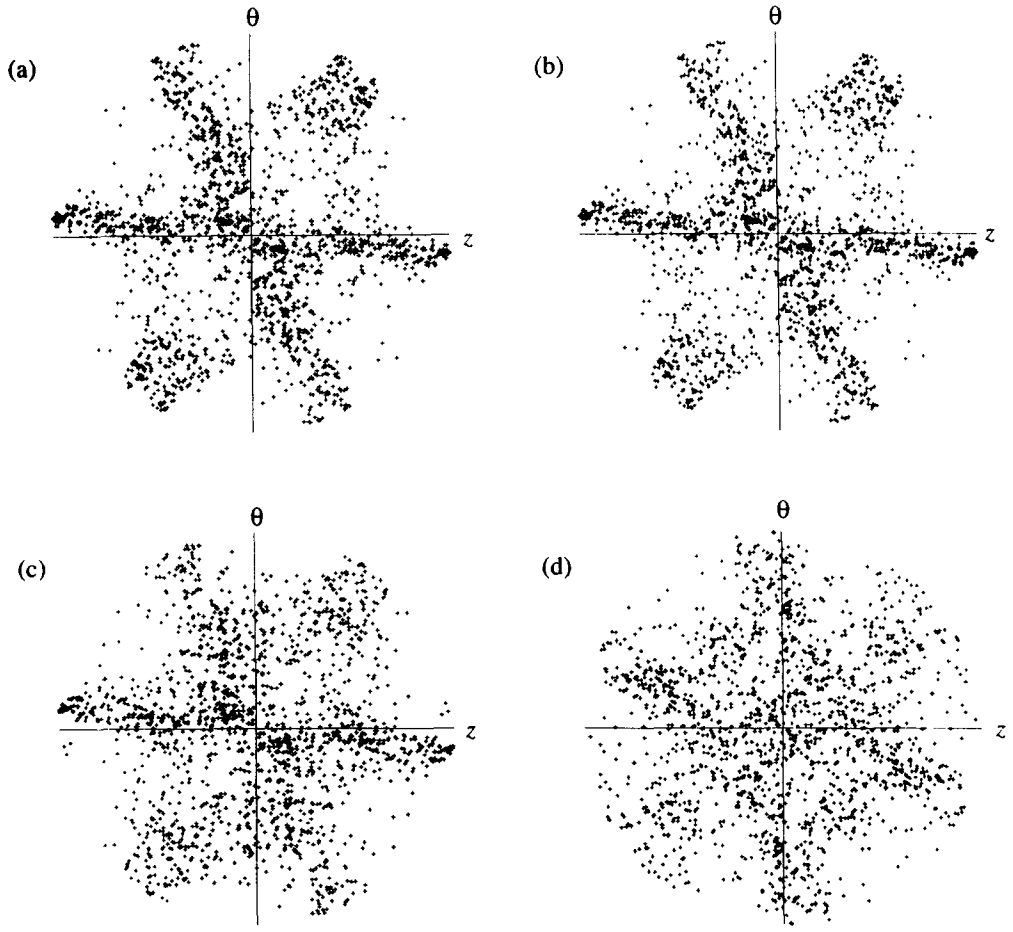

Fig. 10. Predicted {111} pole figures for free-end torsion after forward twisting ($\Gamma = 1.5$) based on the various hardening models: (a) Asaro, (b) Anand, (c) exponential and (d) Bassani–Wu.

It is important to point out that there is no overall consensus in the literature on whether or not the shear texture reverses to a near random state upon reverse deformation. Early work on reverse torsion of copper by Backofen [1950] indicated that reverse torsion did not alter the texture established by the forward twisting. Later, Rollett *et al.* [1988] showed that the texture formed during forward twisting was not simply reversed to the initial state during reverse twisting, but retained maxima with intensities greater than three-times random (see also Lowe & Lipkin [1991]). It seems that the intensities of such resident textures may depend on the amounts of forward torsion before reversal. With very large forward shear $\Gamma = 5.25$ as in Backofen [1950], reverse twisting did not alter the texture established by the forward twisting; with relatively smaller forward shear $\Gamma = 3.5$ as in Rollett *et al.* [1988], a weak resident texture was observed; with even smaller forward shear $\Gamma = 1.5$ as in Anand and Kalidindi [1994], only a very weak resident texture could be restored during reverse twisting. In no case was the resident texture stronger than the texture formed before reversal. It would be worthwhile to systematically study the influence of prestrain on the reversed texture, but this is outside the scope of the present paper.

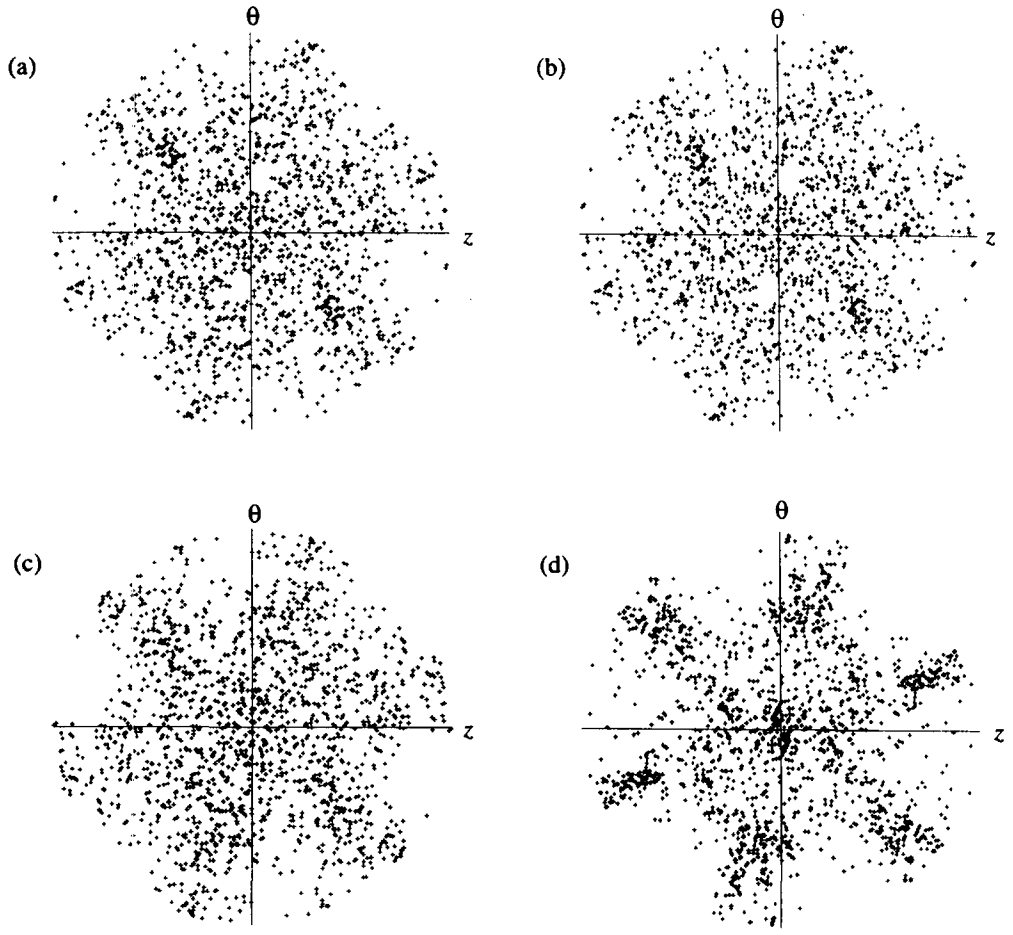

Fig. 11. Predicted {111} pole figures for free-end torsion after complete reverse twisting based on the various hardening models: (a) Asaro, (b) Anand, (c) exponential and (d) Bassani–Wu.

Generally, the Taylor-type polycrystal models together with the finite element method are able to capture the main features of the behaviour of FCC polycrystals during reversed torsion. The small Bauschinger effect observed experimentally can be accurately predicted. Furthermore, the predicted second-order axial effects in the transition region following reversal of the twist direction are in reasonable qualitative agreement with experimental observations. In this respect, it is noted that it is well-known that this transient phenomenon cannot be predicted by macroscopic phenomenological models that do not account for texture development (see e.g. Delhage [1990] and White [1993]), nor by crystal plasticity models neglecting elasticity.

Concerning constitutive models, it is noted that the Bassani–Wu model is considered to be a more physically motivated one than the others considered in this paper. It has been found that only the Bassani–Wu hardening based Taylor-type polycrystal plasticity model qualitatively predicts the experimental shapes of the normal stress curve in fixed-end torsion and the axial strain curve in free-end torsion. However, the predicted texture after reverse twisting based on this model was found to be even stronger than that after forward twisting. One of the possible reasons for this is the use of the Taylor assumption in combination with this hardening model. More detailed studies on the Bassani–Wu hardening model and the validity of the Taylor assumption are in progress and will be reported elsewhere.

Acknowledegments—This work was supported by the Natural Sciences and Engineering Research Council of Canada (NSERC) and the Government of the Province of Quebec (Programme FCAR). P.D. Wu is grateful for the NSERC Canada International Fellowship which supported his postdoctoral position at the Université de Sherbrooke.

REFERENCES

1947 Swift, W., "Length Changes in Metals Under Torsional Overstrain," Engineering, **163**, 253.
1950 Backofen, W. A., "The Torsion Texture of Copper," Trans. AIME, **188**, 1454.
1971 Simmons, G. and Wang, H., Single Crystal Elastic Constants and Calculated Aggregate Properties. The MIT Press, Cambridge.
1981 Chang, Y. W. and Asaro, R. J., "An Experimental Study of Shear Localization in Aluminum–Copper Single Crystals," Acta Metall., **29**, 241.
1984 Peirce, D., Shih, C. F. and Needleman, A., "A Tangent Modulus Method for Rate Dependent Solids," Computers and Structures, **18**, 875.
1985 Asaro, R. J. and Needleman, A., "Texture Development and Strain Hardening in Rate Dependent Polycrystals," Acta Metall., **33**, 923.
1986 Christodoulou, N., Woo, O. T. and MacEwen, S. R., "Effect of Stress Reversals on the Work Hardening Behaviour of Polycrystalline Copper," Acta Metall., **34**, 1553.
1988 Rollett, A. D., Lowe, T., Kocks, U. F. and Stout, M. G., "The Microstructure and Texture of Torsion–Reverse Torsion Experiments," in Kallent, J. S. and Gottstein, G. (eds), Eighth International Conference on Textures of Materials (ICOTOM 8), pp. 473–478.
1989 Brown, S., Kim, K. and Anand, L., "An Internal Variable Constitutive Model for Hot Working Metals" Int. J. Plasticity, **5**, 95.
1989 Harren, S., Lowe, T. C., Asaro, R. J. and Needleman, A., "Analysis of Large-Strain Shear in Rate-dependent Face-centred Cubic Polycrystals: Correlation of Micro- and Macromechanics," Phil. Trans. R. Soc. Lond., **A328**, 443.
1990 Delhage, L., "Strain-rate and Axial Effects During Reversed Large Strain Torsion of Solid Circular Bars," Delft Univ. of Techn., Lab. for Engrg. Mech. Report no. 924.
1990 Field, D. P. and Adams, B. L., "Unrecoverable Strain Hardening in Torsionally Strained OFHC Copper," J. Engng Mater. Technol., **112**, 315.
1990 Neale, K. W., Toth, L. S. and Jonas, J. J., "Large Strain Shear and Torsion of Rate-sensitive FCC Polycrystals," Int. J. Plasticity, **6**, 45.

1991 Bassani, J. L. and Wu, T. Y., "Latent Hardening in Single Crystals II. Analytical Characterization and Predictions," Proc. R. Soc. Lond., **A435**, 21.
1991 Lowe, T. C. and Lipkin, J., "Analysis of Axial Deformation Response During Reverse Shear," J. Mech. Phys. Solids, **39**, 417.
1991 Wu, T. Y., Bassani, J. L. and Laird, C., "Latent Hardening in Single Crystals I. Theory and Experiments," Proc. R. Soc. Lond., **A435**, 1.
1991 Wu, P. D. and Van der Giessen, E., "Analysis of Elastic–Plastic Torsion of Circular Bars at Large Strains," Arch. Appl. Mech., **61**, 89.
1992 Bronkhorst, C. A., Kalidindi, S. R. and Anand, L., "Polycrystalline Plasticity and the Evolution of Crystallographic Texture in FCC Metals," Phil. Trans. R. Soc. Lond., **A341**, 443.
1992 Kalidindi, S. R., Bronkhorst, C. A. and Anand, L., "Crystallographic Texture Evolution in Bulk Deformation Processing of FCC Metals," J. Mech. Phys. Solids, **40**, 537.
1992 Khen. R. and Rubin, M. B., "Analytical Modelling of Second Order Effects in Large Deformation Plasticity," Int. J. Solids Structures, **29**, 2235.
1992a Van der Giessen, E., Neale, K. W. and Qiu, Y., "Analysis of the Swift-effect in Solid Bar Torsion Using a Rate-sensitive Crystal Plasticity Model," in Andersen, S. I. *et al.* (eds), Modelling of Plastic Deformation and Its Applications, pp. 479–483.
1992b Van der Giessen, E., Wu, P. D. and Neale, K. W., "On the Effect of Plastic Spin on Large Strain Elastic–Plastic Torsion of Solid Bars," Int. J. Plasticity, **8**, 773.
1992 White, C. S., "An Analysis of the Thin-walled Torsion Specimen," J. Engng Mater. Technol., **114**, 384.
1993 Van der Giessen, E. and Neale, K. W., "Analysis of the Inverse Swift Effect Using a Rate-sensitive Polycrystal Model," Comp. Meth. Appl. Mech. Engng, **103** 291.
1993 White, C. S., "Reverse Torsion Testing for Material Modeling," J. Mech. Behaviour Mater., **4**, 191.
1993 Wu, P. D. and Van der Giessen, E., "On Large Strain Inelastic Torsion of Glassy Polymers," Int. J. Mech. Sci., **35**, 935.
1994 Anand, L. and Kalidindi, S. R., "The Process of Shear Band Formation in Plane Strain Compression of FCC Metals: Effects of Crystallographic Texture," Mech. Mater., **17**, 223.
1994 Bassani, J. L., "Plastic Flow of Crystals," Adv. Appl. Mech., **30**, 191.
1995 Wu, P. D., Neale, K. W. and Van der Giessen, E., "Length Changes During Large Strain Reverse Torsion," in Advances in Engineering Plasticity and its Applications, T. Abe and T. Tsuta (eds). Pergamon, Amsterdam, pp. 229–234.
1996 Lin, G. and Havner, K. S., "A Comparative Study of Hardening Theories in Torsion Using the Taylor Polycrystal Model," Int. J. Plasticity, **12**, 695.